N-Type Organic Thermoelectrics

Liu, Jian; Qiu, Li; Portale, Giuseppe; Koopmans, Marten; Ten Brink, Gert; Hummelen, Jan C; Koster, L Jan Anton

Published in:
Advanced materials

DOI:
10.1002/adma.201701641

Publication date:
2017

ADVANCED MATERIALS
www.advmat.de

N-Type Organic Thermoelectrics: Improved Power Factor by Tailoring Host–Dopant Miscibility

*Jian Liu, Li Qiu, Giuseppe Portale, Marten Koopmans, Gert ten Brink, Jan C. Hummelen, and L. Jan Anton Koster**

In this contribution, for the first time, the polarity of fullerene derivatives is tailored to enhance the miscibility between the host and dopant molecules. A fullerene derivative with a hydrophilic triethylene glycol type side chain (PTEG-1) is used as the host and (4-(1,3-dimethyl-2,3-dihydro-1H-benzoimidazol-2-yl)phenyl)dimethylamine *n*-DMBI) as the dopant. Thereby, the doping efficiency can be greatly improved to around 18% (<1% for a nonpolar reference sample) with optimized electrical conductivity of 2.05 S cm^{-1}, which represents the best result for solution-processed fullerene derivatives. An in-depth microstructural study indicates that the PTEG-1 molecules readily form layered structures parallel to the substrate after solution processing. The fullerene cage plane is alternated by the triethylene glycol side chain plane; the *n*-DMBI dopants are mainly incorporated in the side chain plane without disturbing the π–π packing of PTEG-1. This new microstructure, which is rarely observed for codeposited thin films from solution, formed by PTEG-1 and *n*-DMBI molecules explains the increased miscibility of the host/dopant system at a nanoscale level and the high electrical conductivity. Finally, a power factor of 16.7 μW m^{-1} K^{-2} is achieved at 40% dopant concentration. This work introduces a new strategy for improving the conductivity of solution-processed n-type organic thermoelectrics.

Organic semiconductors (OSCs) have attracted increasing attention as low-temperature thermoelectric (TE) materials and are promising as low-cost, environmentally benign, large-scale, and mechanically flexible TE modules.[1–7] The energy conversion efficiency of TE materials is defined by the figure-of-merit ZT = $S^2\sigma T/\kappa$, where S is the Seebeck coefficient, σ is the electrical conductivity, T is the absolute temperature, and κ is the thermal conductivity.[8] The thermal conductivity of OSCs is intrinsically low, which leaves the power factor ($S^2\sigma$) as the most important parameter to be optimized for efficient thermoelectrics. Modulating the charge carrier density by doping is considered a key strategy for optimizing the power factor and ZT value.[9–12] Recently, significant progress has been made in p-type organic thermoelectric studies with ZT = 0.42 by using p-type doped conjugated polymers.[13,14] Both efficient p-type and n-type TE materials are required for practical applications. Currently, most of the reported efficient n-type thermoelectric materials are based on n-type doped carbon nanotubes and their composites mixed with polymers.[15–20] However, the development of n-type TE materials based on a single OSC host still lags behind that of their p-type counterparts due to the lack of efficient n-type doped materials.[21–25]

Fullerenes and fullerene derivatives are among best n-type organic semiconductors with high electron mobility and good thermal stability for potential TE applications.[2] The early stage studies focused on doping vacuum-deposited C_{60}, achieving electrical conductivity in the range of 0.05–10 S cm^{-1} and optimized power factor of 12–20.5 μW m^{-1} K^{-2} at room temperature.[26,27] However, these methods are not amenable to solution processing, which is the unique merit of OSCs. Fullerene derivatives with tailorable side chains are excellent n-type OSCs for low-cost TEs. Another merit of fullerene derivatives is the ultralow thermal conductivity (≈0.05 W m^{-1} K^{-1}) in the undoped state due to the modified molecular packing compared to that of C_{60} (≈0.1 W m^{-1} K^{-1}).[28] In 2010, Bao and co-workers reported an efficient and stable n-type dopant, namely, (4-(1,3-dimethyl-2,3-dihydro-1H-benzoimidazol-2-yl)phenyl)dimethylamine (*n*-DMBI) and achieved a conductivity of 1.9×10^{-3} S cm^{-1} by doping solution-processed [6,6]-phenyl-C_{61}-butyric acid methyl ester (PCBM) films.[29] The same group further improved the conductivity of a doped PCBM film to 5.8×10^{-2} S cm^{-1} by tailoring the molecular structure of the dopant.[30] Recently, it was found that fullerene derivatives could also be doped by anion-induced electron transfer from the dopant to the matrix. By using this strategy, conductivities were achieved in the range of 2.5×10^{-3}–3.2×10^{-2} S cm^{-1} in doped PCBM films.[31,32] In general, the doping process of vapor or solution processed organic materials is realized by

Dr. J. Liu, Dr. L. Qiu, Dr. G. Portale, M. Koopmans, G. ten Brink, Prof. J. C. Hummelen, Dr. L. J. A. Koster
Zernike Institute for Advanced Materials
Nijenborgh 4, NL-9747 AG Groningen, The Netherlands
E-mail: l.j.a.koster@rug.nl

Dr. L. Qiu, Prof. J. C. Hummelen
Stratingh Institute for Chemistry
University of Groningen
Nijenborgh 4, NL-9747 AG Groningen, The Netherlands

DOI: 10.1002/adma.201701641

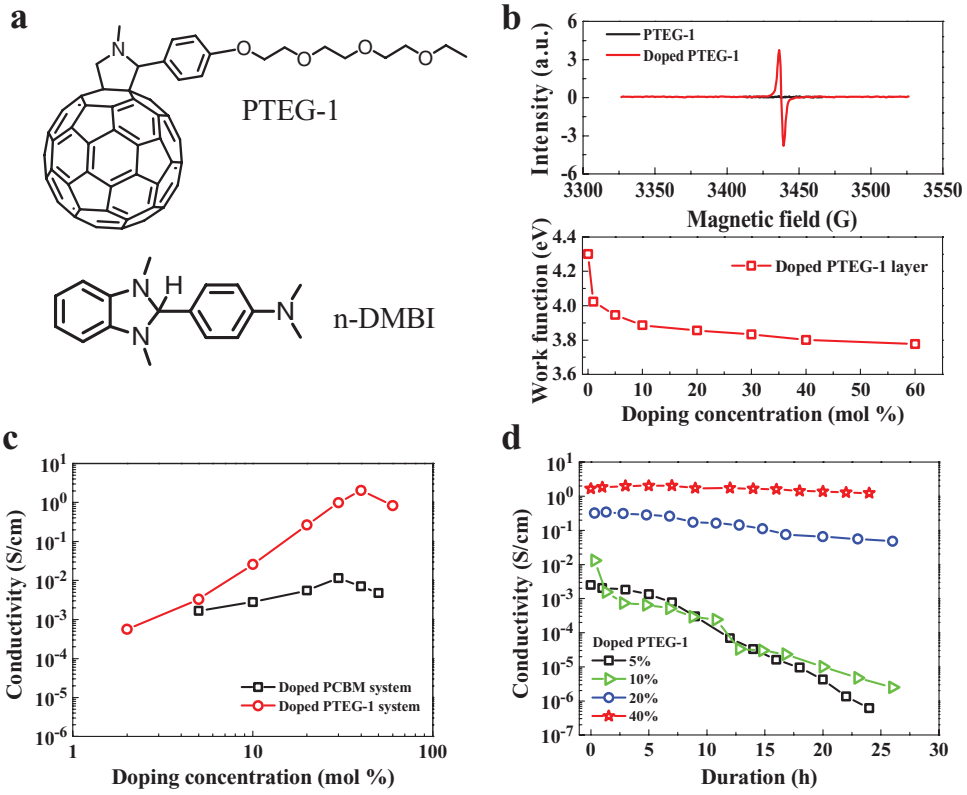

Figure 1. a) The molecular structures of PTEG-1 and *n*-DMBI, b) ESR of pristine and 10% doped PTEG-1 films (upper panel) and work function evolution of pristine and differently doped PTEG-1 films measured by Kelvin probe (lower panel), c) the electric conductivity plotted as a function of doping concentration in doped PCBM and PTEG-1 films, and d) the electric conductivity evolution of doped PTEG-1 films with thermal annealing at 120 °C.

alloying host and dopant molecules in solid films. This method is simple but imposes the challenge of achieving ordered packing of the host molecules. On the other hand, the incorporation of dopant molecules should not increase the system enthalpy much; otherwise phase separation will occur.[33] Such phase segregation in doped films hinders sufficient loading of dopant and thus prevents the further enhancement of electrical conductivity.[23,31] Furthermore, to our knowledge, a TE study of solution-processed fullerene derivatives has not been conducted to date.

In this contribution, we show how carefully tailoring the polarity of organic semiconductors can drastically improve the host/dopant miscibility. We use a fullerene derivative with a hydrophilic triethylene glycol type side chain (PTEG-1) as the host and *n*-DMBI as the dopant with the chemical structures shown in **Figure 1**a. Atomic force microscopy (AFM) and scanning electron microscopy (SEM) studies show that the doped PTEG-1 films did not show an apparent phase separation while many multiscale aggregates were observed on the surface of the less polar PCBM-based system. These results imply an improved host/dopant miscibility for the doped polar PTEG-1 system. As evidenced by grazing-incidence wide-angle X-ray scattering (GIWAXS) study (Figure 3), the PTEG-1 molecules pack in a layered structure with the layers oriented parallel to the substrate and the triethylene glycol type side chain as the interlayer space, and the dopant molecules are preferentially confined in the interlayer space between the C_{60} containing planes. This dopant does not disturb the π–π stacking of host molecules and even improves the ordering of the thin film. Correspondingly, a conductivity of up to 2.05 S cm^{-1} is achieved due to the enhanced doping efficiency, representing the best result for doped solution-processed fullerene derivatives. Finally, a power factor of 16.7 μW m^{-1} K^{-2} is achieved with a Seebeck coefficient of –284 μV K^{-1} at 40% dopant concentration. Our work introduces a new strategy for improving the conductivity of solution-processed n-type organic thermoelectrics.

From the electron-spin resonance (ESR) spectra in the upper panel of Figure 1b, an apparent peak for the polaron charge carriers was observed for the doped PTEG-1 film while the pristine film exhibited a neutral nature. The ESR results confirmed the occurrence of a doping reaction between PTEG-1 and *n*-DMBI molecules. By modulating the doping concentration from 0 to 60 mol%, the work function of doped PTEG-1 films gradually decreased from 4.30 to 3.78 eV as determined by Kelvin probe measurements shown in the bottom panel of Figure 1b. The reduced work function indicated the upward movement of the Fermi level (E_F) in the bandgap and an increased carrier density by adding more dopant.

To characterize the electrical conductivities of the doped films, mixed solutions of PTEG-1 and *n*-DMBI were spin-cast on glass substrates, followed by deposition of narrow and parallel strip Au electrodes as the top contacts. Control devices based on doped PCBM films were also fabricated. The resultant devices were subjected to thermal annealing at 120 °C for 1.5 h. The electrical conductivities of differently doped PTEG-1 and PCBM films were measured and the results are shown in Figure 1c.

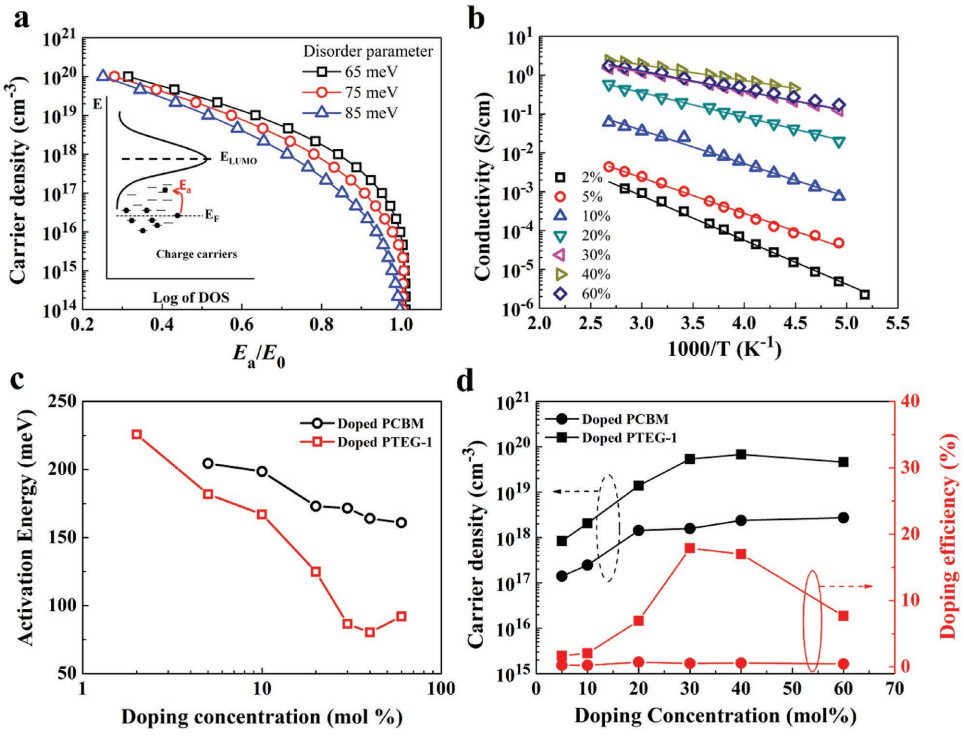

Figure 2. a) Simulated dependence of the relative activation energy E_a/E_0 versus the charge carrier density for different values of the energetic disorder at a temperature range of 260–300 K. The inset shows thermally activated charge transport within the extended Gaussian disorder model. b) The variable temperature conductivities of differently doped PTEG-1 films, and c) the activation energy and d) the estimated carrier density and doping efficiency values of differently doped PCBM and PTEG-1 films.

The doped PCBM film exhibited the best electrical conductivity of 1.16×10^{-2} S cm^{-1} at a doping concentration of 30%, which was higher than the reported value (1.9×10^{-3} S cm^{-1}) obtained for *n*-DMBI doping, probably due to differences in processing.[29] The doped PTEG-1 film exhibited a conductivity similar to that of the doped PCBM film at a low dopant concentration (5%); however, the conductivity of the former increased much faster with the dopant loading and reached its highest value of 2.05 S cm^{-1} at 40%. To our knowledge, this is the highest conductivity reported for solution-processed fullerene derivatives. The high doping of 40% doped PTEG-1 film was confirmed by the independence of the drain–source current on the gate voltage in a transistor device (Figure S1 in the Supporting Information). Further increasing the amount of dopant led to a decrease in conductivity (see Figure 1c). This might have been caused by the disturbing effect of excess dopant molecules on the charge transport network. Figure 1d shows the conductivity evolution with a thermal annealing time at 120 °C for differently doped PTEG-1 films. The doped PTEG-1 films at a doping concentration less than 20 mol% were dedoped quickly by thermal annealing. This dedoping induced by annealing has recently been observed in p-type doped conjugated polymer systems.[34] Surprisingly, the doped PTEG-1 film exhibited a much improved thermal stability by increasing the doping concentration. We speculate that at a high doping concentration the material might be saturated by dopants, and the removal of some excess dopant does not influence the conductivity as much as in low doping systems. In addition, the modification in molecular packing might also contribute to this improvement. Since the thermal stability is another key factor in electronic devices, this unique attribute makes the highly doped PTEG-1 material more promising for practical TE applications.

Because a direct measurement of the charge carrier density in OSCs is difficult due to their low mobility and relatively high energetic disorder, we estimated the carrier density based on the extended Gaussian disorder model (EGDM) reported by Pasveer et al.[35] According to this model, the charge carriers in disordered organic semiconductors hop over an energy landscape with a Gaussian density of states (DOS), which is considered a thermally activated process as schematically shown in the inset of **Figure 2**a. The charge hopping mobility largely depends on the temperature and on the carrier density. Based on the EGDM, we obtained a general relationship between the carrier density and the ratio of activation energy (E_a) to E_0 at different disorder parameters as shown in Figure 2a (see the details in the Supporting Information). Here, E_0 is the activation energy at a low carrier density, which can be obtained from a typical diode measurement. In this modeling, a lattice constant of 1 nm was used for both fullerene derivatives, corresponding to a total DOS of 10^{21} cm^{-3}, and E_0 of 230 meV was used for both PCBM and PTEG-1 films.[36]

To investigate the dependence of the activation energy on the doping process, variable temperature conductivity measurements of various doped films were carried out under vacuum. The results are displayed in Figure 2b and Figure S3 in the Supporting Information. By fitting the temperature dependence of conductivity data with the classic Arrhenius equation, the activation energy values were derived. These are shown in Figure 2c. By controlling the doping concentration from 2 to 40%, the activation energy was changed from 225 to 80 meV. The

reduced activation energy represented a decreased temperature dependence of charge transport at increasing carrier density, which is the essence of the EGDM. We observed an increased activation energy at a doping concentration of 60% with respect to that of the 40% doped sample due to the adverse effect of overloaded dopant. In contrast, the doped PCBM films showed less steep changes (from 205 to 161 meV) in the activation energies in the doping concentration range from 5 to 60%. The smaller activation energy for the doped PTEG-1 films indicated a larger population of charge carriers filling the tail of the DOS compared to the doped PCBM films. The carrier densities were estimated by simply adapting the corresponding E_a/E_0 values of differently doped films to the relationship in Figure 2a and are displayed in Figure 2d. Note that the same disorder parameter (75 meV) was used for both doped PCBM and PTEG-1 thin films according to our previous studies.[37] At low doping concentration, the doping efficiencies are relatively low, which could be a result of the poor thermal stability and Coulomb traps generated by molecular doping.[38,39] As the doping concentration increased the thermal stability was improved and the Coulomb traps disappeared due to the screening effect. The carrier densities increased in and saturated at a certain doping concentration for both doped fullerene derivatives. The saturated carrier densities of doped PTEG-1 films were much higher than those in doped PCBM films, thus explaining the enhanced conductivity. At a doping concentration of 40 mol%, the carrier density in doped PTEG-1 film reached up to 6.8×10^{19} cm^{-3}, falling in the regime ($\approx 10^{19}$–10^{21} cm^{-3}) of the optimal carrier density for thermoelectric applications.[23,40]

The doping efficiency defined by the ratio of carrier density to the number of dopant molecules is regarded as an important parameter to evaluate the quality of the doping process. The peak doping efficiency of 18% was obtained for 30% doping in doped PTEG-1 film. Hence, 18% of the introduced *n*-DMBI molecules were active in the PTEG-1 matrix and are donating electrons to the host molecules. In contrast, a doping efficiency of less than 1% at 30% doping concentration was observed in the doped PCBM system. Note that a similar doping efficiency (around 1%) was recently reported in an n-type conjugated polymer.[23] The remarkably high doping efficiency of doped PTEG-1 films was comparable to that of the p-type organic counterparts.[41] This observation may eventually bring n-type organic thermoelectrics at a level similar to that of the p-type counterparts.

Basically the n-type doping process is related to electron, hydride or H atom transfer from dopant to host; thus the lowest unoccupied molecular orbital (LUMO) level of host molecule with repect to the ionization potential of reducing agent impacts the doping reaction.[21] The possibility of the increased doping efficiency in the doped PTEG-1 system as the result of a modified energy level with respect to PCBM can be excluded because these two fullerene derivatives render similar LUMO levels.[42] To explore the underlying reason, the surface morphologies of pristine and doped films were investigated by AFM and SEM. Figure S4 (Supporting Information) shows topographic AFM images of PCBM and PTEG-1 films before and after doping. The pristine PCBM film exhibited a very smooth surface with a root-mean-square roughness (RMS) of 0.31 nm. After doping, the film became very rough with an RMS roughness of 12.8 nm and many multiscale aggregates were observed on the surface, consistent with a previous study.[43] The *n*-DMBI molecule has a larger polarity than the PCBM matrix (the former is quite soluble in alcohol) and after the doping reaction, the resultant fullerene radical anion (PCBM$^{\bullet}$) renders even larger polarity in the vicinity of the dopant molecule. Consequently, the large polarity difference between the undoped fullerene matrix and the dopant and/or doping products caused the formation of large phase separation, especially after thermal annealing. Different from PCBM, the PTEG-1 molecule contains a basic tertiary amine moiety, which is similar to some structural parts of *n*-DMBI. Furthermore, the hydrophilic triethylene glycol type side chain of the PTEG-1 molecule greatly increases the molecular polarity and is expected to solubilize the doping product. Very recently, ethylene glycol side chains have been used to functionalize conjugated polymers for enhancing their interaction with hydrated ions and water in electrochemical transistor devices and improving the solution coprocessing with p-type dopant in organic p-type doping.[44,45] These studies highlighted the increased polarity by using hydrophilic side chains. Thus, the miscibility between the PTEG-1 matrix and the dopant was improved as evidenced by the AFM morphology shown in Figure S4c,d (Supporting Information) and the SEM study shown in Figure S5 (Supporting Information), where no apparent phase separation was observed upon doping.

In this study, thermal annealing was required to activate the doping reaction and the high electrical conductivity. This might suggest a similar doping mechanism as that proposed by Bao and co-workers.[46] According to their mechanistic study, the rate determining step of electron transfer or hydride transfer pathways of the doping process is highly dependent on the polarity of the environment. Here the PTEG-1 molecule with a polar side chain might provide such polar environment for boosting the doping reaction on the molecular level.

The structure of the pristine and doped PTEG-1 thin films was studied by GIWAXS. 2D-GIWAXS patterns for the pristine and the 40% doped PTEG-1 are shown in **Figure 3**. Both samples showed good ordering, with a well-oriented structure through the whole film, as evidenced by the narrow arc-like signals. In particular, four strong reflections were visible in the 2D-GIWAXS patterns along the near out-of-plane q_z direction (Figure 3a,b). These signals corresponded to the (00*l*) family of reflections and suggested that PTEG-1 adopted a long-range order layered structure along the substrate normal direction. The layer planes contained the fullerene cages and they were oriented parallel to the glass substrate. The spacing extracted from the (001) peak position for the pristine PTEG-1 thin film was 2.2 nm. Because the PTEG-1 molecule is ≈2.15 nm long, interdigitation and tilt of the triethylene glycol ethyl ether side chains are expected. The layered structure readily formed after spin-coating even without annealing (see Figure S6 in the Supporting Information). Layered structures have been reported for other fullerene derivatives.[47,48] Upon annealing, clear off-specular and out-off-plane peaks appeared, suggesting that the molecules tended to pack and form a crystalline structure. However, the order in PTEG-1 remained limited, even after the annealing process (Figure 3a). In contrast, in the presence of the dopant, PTEG-1 showed an improved order, as indicated by the better defined reflections (highlighted in Figure 3b). Interestingly, the (001) peak in the doped PTEG-1 shifted toward lower q_z values, showing an interlayer distance of 2.4 nm and suggesting that the dopant was preferentially included in the interlayer space between the C_{60}

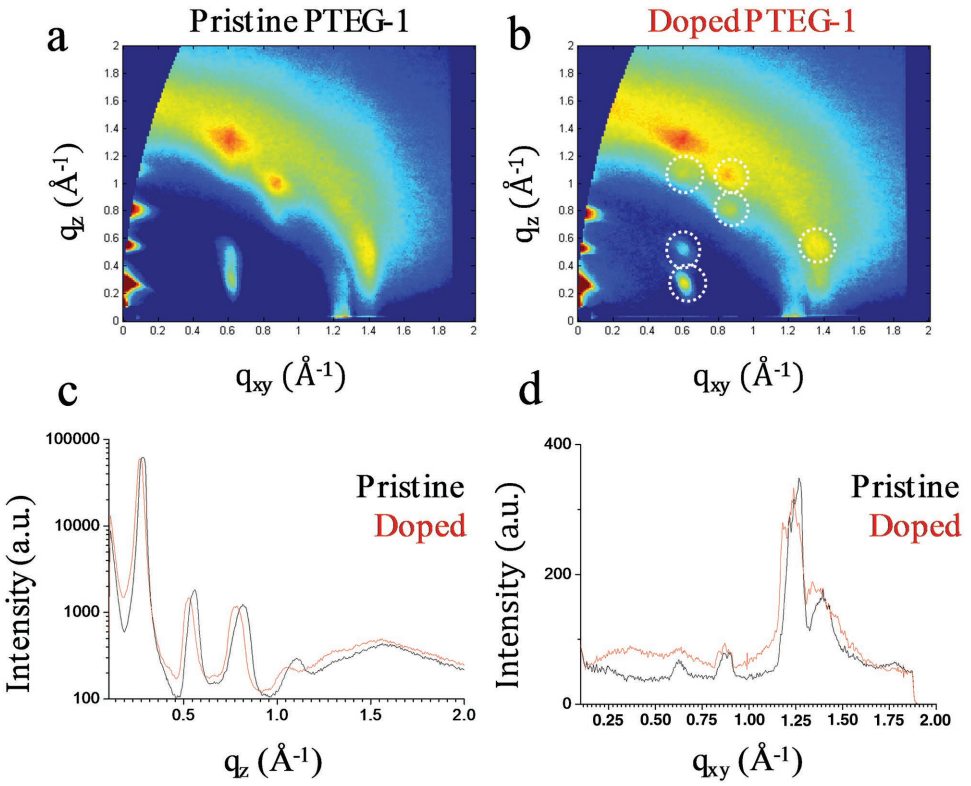

Figure 3. Calibrated 2D GIWAXS patterns for a) pristine PTEG-1 film and b) 40% doped PTEG-1 thin films. The white broken circles highlight the sharper and more intense diffraction spots as a result of molecular doping. c) Near out-of-plane ($q_{xy} \approx 0$) and d) in-plane ($q_z = 0.04$ Å^{-1}) intensity traces for the pristine and 40% doped PTEG-1 thin films. The incident angle used was $\alpha_i = 0.15°$.

containing planes. Moreover, the size of the crystals in the direction perpendicular to the substrate was not apparently changed, with an average value of ≈9 nm after doping (as calculated from the width of the 001 peak). This finding can explain the microstructural origin of increased host/dopant miscibility for doped PTEG-1, and also the increased thermal stability at a high doping concentration. As the order along the q_z and q_{xy} direction was mostly unchanged upon doping (Figure 3c,d), we believed that the dopant had mainly a positive effect on the side chain packing and did not disturb the packing of the fullerene cages. The resultant nanostructure of host/dopant is seldomly seen for codeposited films from solution and is significant for charge transport in terms of efficient doping and molecular ordering.

To evaluate the thermoelectric properties of the doped PTEG-1 films, the Seebeck coefficient was measured in a N_2-filled glove box. A temperature gradient across the sample was imposed by two Peltier devices, and the temperatures of two separate electrodes and the thermal voltage between them were simultaneously probed by two T-type thermocouples (see details in the Experimental Section and Figure S7 in the Supporting Information). By fitting the curves of the thermal voltage versus the temperature gradient, the Seebeck coefficients of doped PTEG-1 films at different doping concentrations were calculated and displayed with the thermoelectric power factor (σS^2), as shown in **Figure 4**a and **Table 1**. Note that the Seebeck coefficient measurement using our method is quite

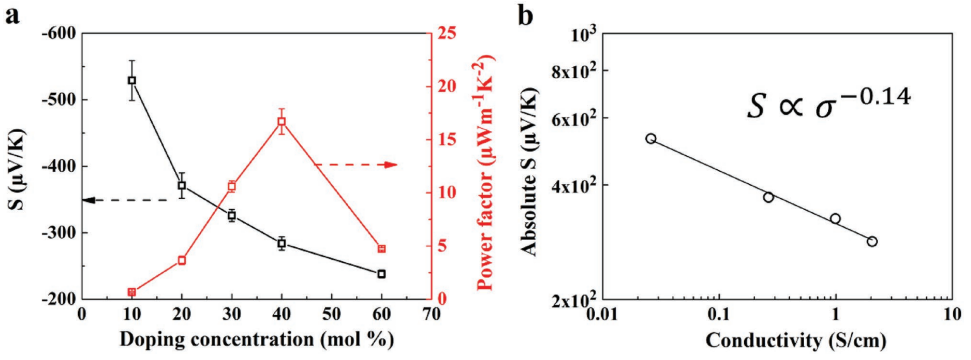

Figure 4. a) The measured Seebeck coefficient (*S*, black line) and power factor (red line) values in differently doped PTEG-1 films and b) correlation of the Seebeck coefficient with conductivity obtained from the experimental data.

Table 1. Thermoelectric parameters of the differently doped PTEG-1 films with reference to doped PCBM film at room temperature.

Sample	Dopant weight [mol%]	σ [S cm^{-1}]	E_A [meV]	n [cm^{-3}]	S [μV K^{-1}]	σS^2 [μW m^{-1} K^{-2}]
PCBM	30	0.012	172	2.4×10^{18}	−248 ± 20	0.08
PTEG-1	10	0.026	170	2.1×10^{18}	−529 ± 30	0.73 ± 0.08
	20	0.265	125	1.4×10^{19}	−371 ± 19	3.66 ± 0.39
	30	0.993	86.5	5.4×10^{19}	−326 ± 9	10.6 ± 0.53
	40	2.05	80.3	6.8×10^{19}	−284 ± 10	16.7 ± 1.2
	60	0.835	92	4.6×10^{19}	−238 ± 6	4.74 ± 0.12

reliable with small sample-to-sample variation and negligible contact geometry effect (see details in the Supporting Information). At a doping concentration of 10%, the doped PTEG-1 film showed a large S of −529 ± 30 μV K^{-1}. The negative sign of S agreed with the n-type doping of the film. As the doping concentration increased, the absolute S decreased while the conductivity σ increased. As a result, the best thermoelectric power factor of 16.7 ± 1.2 μW m^{-1} K^{-2} with a S of −284 ± 10 μV K^{-1} was obtained at a doping concentration of 40%. To our knowledge, this is the best reported power factor value for a solution-processed fullerene derivative based film and represents one of the best results for n-type organic thermoelectric materials.[18,19,21] The reference sample of 30% doped PCBM film showed a Seebeck coefficient of −248 ± 20 μV K^{-1}. However, due to the poor morphology resulting from the bad miscibility, the electrical conductivity σ was greatly suppressed, which led to an extremely low power factor of 0.08 μW m^{-1} K^{-2} as listed in Table 1.

In general, the Seebeck coefficient of disordered organic semiconductors results from the thermal activation of charge transport. Thus, the activation energy (E_S) based on the Seebeck coefficient can be derived from the following formula[27]

$$E_S = |S| \cdot T \cdot e. \quad (1)$$

The E_S value of 40% doped PTEG-1 film was ≈83 meV, i.e., very close to the E_a (80.3 meV) obtained from variable temperature conductivity. Such an agreement between E_a and E_S has also been seen in evaporated doped C_{60} films with high molecular order, but is rarely observed in solution-processed films.[23,25,27] However, we observed a large discrepancy between E_a and E_S in 60% doped PTEG-1 film, confirming the negative effect of overloaded dopant on the charge transport.[27] Previous studies reported that the variation of S as a function of σ followed an empirical relation of $S \propto \sigma^{-0.25}$ in doped semiconducting polymers.[25,49] The dopant was reported to be intercalated between π-stacking conjugated chains in the codeposited films of conjugated polymers from solution.[34,50] Interestingly, the doped PTEG-1 did not follow this trend (see Figure 4b). The slow decrease of absolute S with increasing σ eventually led to a high power factor as observed in the doped PTEG-1 system.

In summary, we demonstrated a promising n-type doped system for organic thermoelectrics by tailoring the host–dopant miscibility. A polar fullerene derivative (PTEG-1) was doped by the commonly used *n*-DMBI dopant with a doping efficiency of up to 18%. The dopant molecules were mainly confined in the interlayer space consisting of triethylene glycol-type side chains and did not disturb π–π stacking of PTEG-1 molecules, leading to good host/dopant miscibility. As a result, a very high electrical conductivity of 2.05 S cm^{-1} was realized at a doping concentration of 40%, which represents the best result for solution-processed doped fullerene derivative films. Interestingly, it was found that the thermal stability of the doped PTEG-1 system could be improved by increasing the amount of dopant. The optimized power factor of 16.7 μW m^{-1} K^{-2} was achieved with a Seebeck coefficient of −284 μV K^{-1} at 40% doping concentration, which was comparable to the best results obtained with vacuum-deposited doped fullerene films. Our work points out the direction to advance the development of efficient n-type organic thermoelectrics.

Experimental Section

Materials: PETG-1 was synthesized according to a previously reported procedure.[42] *n*-DMBI was purchased from Sigma Aldrich.

Device Fabrication: The borosilicate glass substrates were sequentially washed using detergent, acetone, and isopropanol. Then, the substrates were dried using a nitrogen gun and treated by UV–ozone for 20 min. The doped PTEG-1 films were prepared by spin-coating PTEG-1 solution (5 mg mL^{-1} in chloroform) mixed with different amounts of dopant solution (5 mg mL^{-1} in chloroform) in a glove box with nitrogen atmosphere. The film thickness (d) was between 40 and 50 nm. For the electrical conductivity measurements, parallel line-shape Au electrodes with a width (w) of 13 mm and a channel length (L) of 100–300 μm were deposited as the top contact. Voltage-sourced two-point conductivity measurements were conducted in a probe station in a N_2 glove box and variable temperature conductivity was measured under vacuum in a cryogenic probe station. The electrical conductivity (σ) was calculated according to the formula: $\sigma = (J/V) \times L/(w \times d)$. The conductivity of commercial PEDOT:PSS (Clevios P VP AI 4083) was measured to be 0.06 S m^{-1}, which was consistent with the standard value of 0.02–0.2 S m^{-1}.

Characterization of Thin Films: The thicknesses of all films were measured by ellipsometry. AFM topographical images were recorded in tapping mode using a Bruker MultiMode 8 microscope with TESP probes. SEM topographical images were recorded on an XL 30 ESEM microscope. The work function of pristine and doped PTEG-1 films spin-coated on a 30 nm Au layer, was determined by a Kelvin probe station (Besocke Delta Phi) with standard HOPG as the reference sample (work function = 4.6 eV).

The Seebeck coefficient was measured using a home-built setup (see details in the Supporting Information) and a continuously changed temperature gradient was imposed across the devices to measure the thermal voltage at varying temperature differences.

GIWAXS measurements were performed at the Duthc-Belgian beamline (DUBBLE) BM26B at the European Synchrotron Radiation Facility (ESRF), Grenbole, France.[51,52] An X-ray beam with energy of 12 keV (λ = 1.033 Å) was used with a sample-to-detector distance of 150 mm. GIWAXS frames were collected using a Frelon CCD camera and using an exposure time of 30 s per frame. All the necessary corrections for GIWAXS data have been taken into account (detector efficiency, flat field, solid angle, and polarization).[53] The beam centre was estimated using the known postion of diffracted rings from standard Silver Behenate and α-Al_2O_3 powders. The scattering vector q was defined with respect to the center of the incident beam and has a

magnitude of $q = (4\pi/\lambda)\sin(\theta)$, where 2θ is the scattering angle and λ is the wavelength of the X-ray beam. Herein we opted to present the wedge-shaped corrected images where q_{xy} and q_z are the in-plane and near out-of-plane scattering vectors, respectively. The scattering vectors are defined as follows: $q_x = (2\pi/\lambda)(\cos(2\theta_f)\cos(\alpha_f)\text{-}\cos(\alpha_i))$, $q_y = (2\pi/\lambda)(\sin(2\theta_f)\cos(\alpha_f))$, $q_z = (2\pi/\lambda)(\sin(\alpha_f) + \sin(\alpha_i))$, $q_{xy}^2 = q_x^2 + q_y^2$, where α_f is the exit angle in the vertical direction and $2\theta_f$ is the in-plane scattering angle, in agreement with standard GIWAXS notation.[54] An incident angle $\alpha_i = 0.15°$ has been used for all the samples.

Supporting Information

Supporting Information is available from the Wiley Online Library or from the author.

Acknowledgements

The authors thank Arjen Kamp for the technical support in building the Seebeck setup. This is a publication by the FOM Focus Group "Next Generation Organic Photovoltaics," participating in the Dutch Institute for Fundamental Energy Research (DIFFER).

Conflict of Interest

The authors declare no conflict of interest.

Keywords

conductivity, fullerene derivatives, n-type doping, organic thermoelectrics

Received: March 23, 2017
Revised: May 22, 2017
Published online: July 19, 2017

[1] M. Culebras, C. Gómez, A. Cantarero, *Materials* **2014**, *7*, 6701.
[2] J. Yang, H.-L. Yip, A. K.-Y. Jen, *Adv. Energy Mater.* **2013**, *3*, 549.
[3] T. O. Poehler, H. E. Katz, *Energy Environ. Sci.* **2012**, *5*, 8110.
[4] B. T. McGrail, A. Sehirlioglu, E. Pentzer, *Angew. Chem., Int. Ed. Engl.* **2015**, *54*, 1710.
[5] L. E. Bell, *Science* **2008**, *321*, 1457.
[6] J. R. Sootsman, D. Y. Chung, M. G. Kanatzidis, *Angew. Chem., Int. Ed.* **2009**, *48*, 8616.
[7] R. Kroon, D. A. Mengistie, D. Kiefer, J. Hynynen, J. D. Ryan, L. Yu, C. Müller, *Chem. Soc. Rev.* **2016**, *45*, 6147.
[8] O. Bubnova, Z. U. Khan, A. Malti, S. Braun, M. Fahlman, M. Berggren, X. Crispin, *Nat. Mater.* **2011**, *10*, 429.
[9] O. Bubnova, M. Berggren, X. Crispin, *J. Am. Chem. Soc.* **2012**, *134*, 16456.
[10] T. Menke, D. Ray, H. Kleemann, K. Leo, M. Riede, *Phys. Status Solidi* **2015**, *252*, 1877.
[11] O. Bubnova, Z. U. Khan, A. Malti, S. Braun, M. Fahlman, M. Berggren, X. Crispin, *Nat. Mater.* **2011**, *10*, 429.
[12] K. P. Pernstich, B. Rössner, B. Batlogg, *Nat. Mater.* **2008**, *7*, 321.
[13] G.-H. Kim, L. Shao, K. Zhang, K. P. Pipe, *Nat. Mater.* **2013**, *12*, 719.
[14] Z. Fan, P. Li, D. Du, J. Ouyang, *Adv. Energy Mater.* **2017**, *7*, 1602116.
[15] T. Fukumaru, T. Fujigaya, N. Nakashima, U. Dettlaff-Weglikowska, S. Roth, *Sci. Rep.* **2015**, *5*, 7951.
[16] Y. Nonoguchi, K. Ohashi, R. Kanazawa, K. Ashiba, K. Hata, T. Nakagawa, C. Adachi, T. Tanase, T. Kawai, *Sci. Rep.* **2013**, *3*, 1228.
[17] C. Cho, M. Culebras, K. L. Wallace, Y. Song, K. Holder, J.-H. Hsu, C. Yu, J. C. Grunlan, *Nano Energy* **2016**, *28*, 426.
[18] H. Wang, J.-H. Hsu, S.-I. Yi, S. L. Kim, K. Choi, G. Yang, C. Yu, *Adv. Mater.* **2015**, *27*, 6855.
[19] C. Cho, K. L. Wallace, P. Tzeng, J.-H. Hsu, C. Yu, J. C. Grunlan, *Adv. Energy Mater.* **2016**, *6*, 1502168.
[20] C. Yu, A. Murali, K. Choi, Y. Ryu, T. Plocke, J. Maultzsch, C. Thomsen, F. Hauke, A. Hirsch, U. J. Kim, E. H. Lee, H. J. Shin, J. Y. Choi, Y. H. Lee, *Energy Environ. Sci.* **2012**, *5*, 9481.
[21] K. Shi, F. Zhang, C.-A. Di, T.-W. Yan, Y. Zou, X. Zhou, D. Zhu, J.-Y. Wang, J. Pei, *J. Am. Chem. Soc.* **2015**, *137*, 6979.
[22] B. Russ, M. J. Robb, F. G. Brunetti, P. L. Miller, E. E. Perry, S. N. Patel, V. Ho, W. B. Chang, J. J. Urban, M. L. Chabinyc, C. J. Hawker, R. A. Segalman, *Adv. Mater.* **2014**, *26*, 3473.
[23] R. A. Schlitz, F. G. Brunetti, A. M. Glaudell, P. L. Miller, M. A. Brady, C. J. Takacs, C. J. Hawker, M. L. Chabinyc, *Adv. Mater.* **2014**, *26*, 2825.
[24] C. Mai, R. A. Schlitz, G. M. Su, D. Spitzer, X. Wang, S. L. Fronk, D. G. Cahill, M. L. Chabinyc, G. C. Bazan, *J. Am. Chem. Soc.* **2014**, *136*, 13478.
[25] S. Wang, H. Sun, U. Ail, M. Vagin, P. O. Å. Persson, J. W. Andreasen, W. Thiel, M. Berggren, X. Crispin, D. Fazzi, S. Fabiano, *Adv. Mater.* **2016**, *28*, 10764.
[26] M. Sumino, K. Harada, M. Ikeda, S. Tanaka, K. Miyazaki, C. Adachi, *Appl. Phys. Lett.* **2011**, *99*, 93308.
[27] T. Menke, D. Ray, J. Meiss, K. Leo, M. Riede, *Appl. Phys. Lett.* **2012**, *100*, 93304.
[28] X. Wang, C. D. Liman, N. D. Treat, M. L. Chabinyc, D. G. Cahill, *Phys. Rev. B* **2013**, *88*, 075310.
[29] P. Wei, J. H. Oh, G. Dong, Z. Bao, *J. Am. Chem. Soc.* **2010**, *132*, 8852.
[30] B. D. Naab, S. Zhang, K. Vandewal, A. Salleo, S. Barlow, S. R. Marder, Z. Bao, *Adv. Mater.* **2014**, *26*, 4268.
[31] C.-Z. Li, C.-C. Chueh, F. Ding, H.-L. Yip, P.-W. Liang, X. Li, A. K.-Y. Jen, *Adv. Mater.* **2013**, *25*, 4425.
[32] C.-Z. Li, C.-C. Chueh, H.-L. Yip, F. Ding, X. Li, A. K.-Y. Jen, *Adv. Mater.* **2013**, *25*, 2457.
[33] J. W. Cahn, *J. Chem. Phys.* **1965**, *42*, 93.
[34] K. Kang, S. Watanabe, K. Broch, A. Sepe, A. Brown, I. Nasrallah, M. Nikolka, Z. Fei, M. Heeney, D. Matsumoto, K. Marumoto, H. Tanaka, S.-I. Kuroda, H. Sirringhaus, *Nat. Mater.* **2016**, *15*, 896.
[35] W. F. Pasveer, J. Cottaar, C. Tanase, R. Coehoorn, P. A. Bobbert, P. W. M. Blom, D. M. de Leeuw, M. A. J. Michels, *Phys. Rev. Lett.* **2005**, *94*, 206601.
[36] N. I. Craciun, J. Wildeman, P. W. M. Blom, *Phys. Rev. Lett.* **2008**, *100*, 56601.
[37] S. Torabi, F. Jahani, I. van Severen, C. Kanimozhi, S. Patil, R. W. A. Havenith, R. C. Chiechi, L. Lutsen, D. J. M. Vanderzande, T. J. Cleij, J. C. Hummelen, L. J. A. Koster, *Adv. Funct. Mater.* **2015**, *25*, 150.
[38] A. Abate, D. R. Staff, D. J. Hollman, H. J. Snaith, A. B. Walker, B. D. Naab, J. Q. Zhong, J. Park, W. Chen, Y. Cui, *Phys. Chem. Chem. Phys.* **2014**, *16*, 1132.
[39] V. I. Arkhipov, E. V. Emelianova, P. Heremans, H. Bässler, *Phys. Rev. B* **2005**, *72*, 235202.
[40] G. J. Snyder, E. S. Toberer, *Nat. Mater.* **2008**, *7*, 105.
[41] P. Pingel, M. Arvind, L. Kölln, R. Steyrleuthner, F. Kraffert, J. Behrends, S. Janietz, D. Neher, *Adv. Electron. Mater.* **2016**, *2*, 1600204.
[42] F. Jahani, S. Torabi, R. C. Chiechi, L. Jan, A. Koster, J. C. Hummelen, *Chem. Commun.* **2014**, *50*, 10645.
[43] P. Wei, T. Menke, B. D. Naab, K. Leo, M. Riede, Z. Bao, *J. Am. Chem. Soc.* **2012**, *134*, 3999.

[44] A. Giovannitti, C. B. Nielsen, D.-T. Sbircea, S. Inal, M. Donahue, M. R. Niazi, D. A. Hanifi, A. Amassian, G. G. Malliaras, J. Rivnay, I. McCulloch, *Nat. Commun.* **2016**, *7*, 13066.
[45] R. Kroon, D. Kiefer, D. Stegerer, L. Yu, M. Sommer, C. Müller, *Adv. Mater.* **2017**, DOI: 10.1002/adma.201700930.
[46] B. D. Naab, S. Guo, S. Olthof, E. G. B. Evans, P. Wei, G. L. Millhauser, A. Kahn, S. Barlow, S. R. Marder, Z. Bao, *J. Am. Chem. Soc.* **2013**, *135*, 15018.
[47] X. Zhang, X.-D. Li, L.-X. Ma, B. Zhang, *RSC Adv.* **2014**, *4*, 60342.
[48] M. J. Hollamby, M. Karny, P. H. H. Bomans, N. A. J. M. Sommerdjik, A. Saeki, S. Seki, H. Minamikawa, I. Grillo, B. R. Pauw, P. Brown, J. Eastoe, H. Möhwald, T. Nakanishi, *Nat. Chem.* **2014**, *6*, 690.
[49] A. M. Glaudell, J. E. Cochran, S. N. Patel, M. L. Chabinyc, *Adv. Energy Mater.* **2015**, *5*, 1401072.
[50] H. Méndez, G. Heimel, S. Winkler, J. Frisch, A. Opitz, K. Sauer, B. Wegner, M. Oehzelt, C. Röthel, S. Duhm, D. Többens, N. Koch, I. Salzmann, *Nat. Commun.* **2015**, *6*, 8560.
[51] W. Bras, I. P. Dolbnya, D. Detollenaere, R. van Tol, M. Malfois, G. N. Greaves, A. J. Ryan, E. Heeley, *J. Appl. Crystallogr.* **2003**, *36*, 791.
[52] G. Portale, D. Cavallo, G. C. Alfonso, D. Hermida-Merino, M. van Drongelen, L. Balzano, G. W. M. Peters, J. G. P. Goossens, W. Bras, *J. Appl. Crystallogr.* **2013**, *46*, 1681.
[53] P. Müller-Buschbaum, *Adv. Mater.* **2014**, *26*, 7692.
[54] G. Renaud, R. Lazzari, F. Leroy, *Surf. Sci. Rep.* **2009**, *64*, 255.